Biophysical effects of afforestation on land surface temperature in Guangdong Province, southern China

Wenjuan Shen[1,2], Jiaying He[3], Tao He[4], Xiangping Hu[5], Xin Tao[6], and Chengquan Huang[7]

[1] College of Forestry, Nanjing Forestry University, Nanjing 210037, China.

[2] Co-Innovation Center for Sustainable Forestry in Southern China, Nanjing Forestry University, Nanjing 210037, China.

[3] Department of Earth System Science, Tsinghua University, Beijing 100084, China.

[4] School of Remote Sensing and Information Engineering, Wuhan University, Hubei 430079, China.

[5] Industrial Ecology Programme, Department of Energy and Process Engineering, Norwegian University of Science and Technology (NTNU), Trondheim 7491, Norway.

[6] Department of Geography, University at Buffalo, Buffalo, NY 14261, USA.

[7] Department of Geographical Sciences, University of Maryland, College Park, MD 20742, USA.

Corresponding author: Wenjuan Shen (wjshen@njfu.edu.cn)

Key Points:

- The modeled land surface temperature due to afforestation had a net warming effect.
- The non-radiative process mainly drives the effect of afforestation on local surface temperature.
- The detailed distribution of afforestation and a precise energy balance model allow accurate evaluation of the temperature response.

Abstract

Developing effective climate mitigation strategies under global warming requires a comprehensive understanding of the biophysical mechanism of how afforestation affects the climate and environment. The planted forests in southern China are an essential carbon sink. However, the impacts of radiative and non-radiative processes on land surface temperature caused by converting open land (i.e., grassland and cropland) and natural forests to planted forests remain unclear. We used satellite observations and intrinsic biophysical mechanism theory-based energy balance models to estimate the biophysical impacts of potential afforestation of open land and natural forests on surface temperature from 2000 to 2010 in Guangdong Province, southern China. Results showed that afforestation of open land had a consistent net cooling effect. Due to the afforestation of natural forests, the modeled results revealed that afforestation among all conversion types had a net warming effect of 0.15±0.5 K, which caused by the change in energy redistribution factor although uncertainty remains. While the most significant warming caused by converting natural forest to planted forests was also slightly affected by albedo. The afforestation's non-radiative and radiative processes led to a slight warming of 0.143±0.43 K and a cooling of −0.096±0.19 K, respectively. The non-radiative process dominates the effect of afforestation on the surface temperature, with the overall non-radiative forcing index greater than 73%±0.59%. Our study highlights the need of protecting natural forests and provides a practical method for assessing the impacts of afforestation on the local climate and the effectiveness of climate mitigation efforts.

Plain Language Summary

Afforestation is an important tool for mitigating climate change. However, the land cover change induced by afforestation may affect the land-atmosphere balance of water and energy. Accurate estimation of surface temperature change in response to afforestation-induced surface energy change is challenging. From 2000 to 2010, afforestation activities in southern China were frequent, resulting in a significant increase in carbon sinks. Yet, how these land-use changes can affect the local climate is unclear. Here we prepared the high-resolution land cover data and utilized satellite observations and a physical-based method to estimate the impacts of afforestation on land surface temperature in southern China. This strategy can provide insights for designing rational afforestation policies in southern China and similar geographic areas.

1. Introduction

Afforestation is typically referred to as a human-driven process of seedling or planting new forests on land that has been absent from forests for at least 50 years in the past (Brown et al., 1986; Lund, 2006). Land use and land cover change (LULCC) driven by afforestation can affect the carbon budget and surface energy balance of local ecosystems through biogeophysical and biogeochemical processes, which will further influence the climate change from regional to global scales (Anderson et al., 2011; Bonan, 2008; Duveiller et al., 2018). In particular, the biophysical processes related to afforestation can control the land-atmospheric exchange of water and energy by altering the radiative (e.g. albedo) and non-radiative (e.g. evapotranspiration and roughness) characteristics (Alkama and Cescatti, 2016; Bright et al., 2017; Huang et al., 2020; Zhao and Jackson, 2014). This will further affect surface energy redistributions and exert warming or cooling effects on the local climate (Bright et al., 2017). For example, the non-radiative effects of forest gains dominate the local response and lead to cooling in most regions experiencing disturbances across the world (Bright et al., 2017). However, a comprehensive evaluation of how forest change affects regional temperature through the radiative and non-radiative processes is still lacking in afforested areas, normally referred to as planted forests (PF). Accurate quantification of afforestation impacts on land surface temperature (LST) is also challenging due to the lack of long-term land records at high resolution for capturing the spatiotemporal distribution of afforestation (Li et al., 2016; Prevedello et al., 2019). Moreover, it remains unclear that afforestation induces the surface temperature changes through which biophysical variables at a regional scale (Li et al., 2015; Peng et al., 2014; Prevedello et al., 2019).

The biophysical impacts of forest change on LST are typically evaluated using in situ meteorological observations, remote sensing data, or climate models (Chen and Dirmeyer, 2020; Li et al., 2022; Mahmood et al., 2014). Although in situ measurements provide direct and accurate observations for studying such impacts, they are limited in spatial coverages and lack mechanical explanations (Senior et al., 2017). Climate models can account for both biophysical and external atmospheric feedbacks, but their performances are affected by various types of uncertainties (He et al., 2015; Wickham et al., 2013; Yu et al., 2015). Empirical models with remote sensing observations have become a primary tool for analyzing the relationships between forest cover and climate at the regional and global scales (Li et al., 2016; Peng et al., 2014). Existing studies have explored the impact of afforestation on LST using various remote sensing datasets (Li et al., 2016; Prevedello et al., 2019; Shen et al., 2020; Shen et al., 2019b). For example, Ge et al. (2019) have analyzed the climate feedback of afforestation in China based on Moderate-Resolution Imaging Spectroradiometer (MODIS) land cover data. Yet, the coarse-resolution MODIS land cover data may easily affect the results in heterogeneous areas with mixed land cover pixels (Novo-Fernández et al., 2018). Also, few studies have investigated how biophysical energy balance mechanisms, such as albedo radiation feedbacks and energy redistribution changes, drive afforestation-induced temperature change in southern China using high-resolution LULCC data.

Energy balance models based on different physical theories have been developed to evaluate the impacts of LULCC on the climate (Li et al., 2020; Liao et al., 2018; Luyssaert et al., 2014; Rigden and Li, 2017; Wang et al., 2018). Specifically, the intrinsic biophysical mechanism (IBM) theory is a commonly adopted method to quantify the biophysical impacts of land-use change on the LST (Lee et al., 2011). The energy balance model based on the IBM theory is capable of distinguishing between internal forcing and external feedback of LULCC and has been used to separate the effects of the radiative and non-radiative processes induced by afforestation on the LST (Lee et al., 2011). As in situ measurements, such as FLUXNET and meteorological observations, can provide accurate values of these intrinsic biophysical parameters, many researchers are trying to scale them to larger scales to study the non-radiative mechanisms induced by afforestation through the combination of energy balance models (Bright et al., 2017; Ge et al., 2019). Nevertheless, this method is limited due to the sparse distribution of in situ observations (Tang et al., 2018; Wang et al., 2018). This can be addressed by utilizing remote sensing data with spatial consistency. Thus, a combination of remote sensing observations, in situ measurements, and energy balance models can provide a new direction for assessing the impacts of forest changes and their biophysical characteristics on surface temperature (Bright et al., 2017; Ge et al., 2019).

Afforested areas in southern China play a critical role in driving LULCC and restoring total vegetation carbon storage in China. Afforestation projects, such as converting from croplands to forests, have been continuously increasing during the recent years. Economic demands have promoted substantial conversion from natural forests (NF) into commercial forests in this region, especially between 2000 and 2010 (Shen et al., 2018; Shen et al., 2019b). Driven by the market, fast-growing and high-yield tree species have commonly used in some projects as they can quickly grow into forests in a short-rotation period. As a result, the mixed forest species with NF areas have been gradually replaced by monospecific even-aged plantations in southern China, particularly Guangdong province. Nevertheless, the biophysical impacts of these afforestation practices on LST in southern China are still poorly understood.

This study aims to estimate the biophysical impacts of afforestation on the local surface temperature from 2000 to 2010 across Guangdong Province, southern China. We quantified the response of LST to afforestation using both satellite observations and a physical-based method that integrates the energy balance model and IBM theory. We also assessed the radiative and non-radiative effects of afforestation in our study area. Specifically, we compared the differences between afforested areas and the NF, and assessed the afforestation impacts in open land areas, including cropland (CR) and grassland (GR).

2. Materials and Methods

2.1. Data preparation

The distributions of PF, NF, and open land (CR and GR) areas in 2000 and 2010 in Guangdong Province were identified from two 30m land cover datasets: SGB-NDVI-based forest and non-forest (FNF) time series maps (Shen et al., 2019a) and GlobeLand30 data product (Chen et al., 2015). The accuracy of the SGB-NDVI-based FNF and GlobeLand30 ranged from 83%-86% (Shen et al., 2019a) and 84%-89% (Chen et al., 2015), respectively. We first mapped the PF and non-forest areas using the dense time series SGB-NDVI-based FNF data. Here we defined the PF as the intersection between non-forest from the year before the current year (i.e., persisting non-forest or deforestation in 2009) and the forest in the current year (i.e., afforestation or post-deforestation reforestation in 2010) following previous studies (Shen et al., 2019a,b). The GlobeLand30 data was then used to identify the NF (forest minus PF), CR and GR areas, as described in Shen et al. (2019b). The total area of the mapped PF is close to that from the National Forestry Yearbook of China (Shen et al., 2019b). To assess the impacts of the potential afforestation across space and time, the pixels that did not experience changes in land cover types between 2000 and 2010 were then used as reference pixels for comparisons. We further resampled the original values from 30m resolution to 1km using the nearest neighbor method to match the biophysical variables from the MODIS data.

Biophysical and climatic variables were primarily obtained from MODIS products (Table 1). We acquired the LST data from the 8-day MODIS MYD11A2 product, the albedo data from the MCD43B3 product, the MOD16A2 evapotranspiration (ET) data, the downward longwave surface fluxes from GLASS LW_modis data provided by the National Earth System Science Data Center (http://www.geodata.cn), and the downward shortwave surface fluxes from the 3-hours MODIS MCD18A1 product. We then extracted the monthly and seasonal averages of the variables for all these datasets. The monthly air temperatures at 2m above the ground were also obtained from the China Meteorological Data service center (http://data.cma.cn/en) as a reference. These in-situ measurements covering 26 meteorological stations were interpolated using the random forest models developed by Shen et al. (2019b). The interpolated and observed

2m air temperature showed a strong correlation, with Pearson's r values ranging between 0.8 to 0.99 for the 2000 and 2010 data (Shen et al., 2019b). We then generated the daily, monthly, and annual averages of the LST and calculated the annual and monthly averages of the in-situ air temperature.

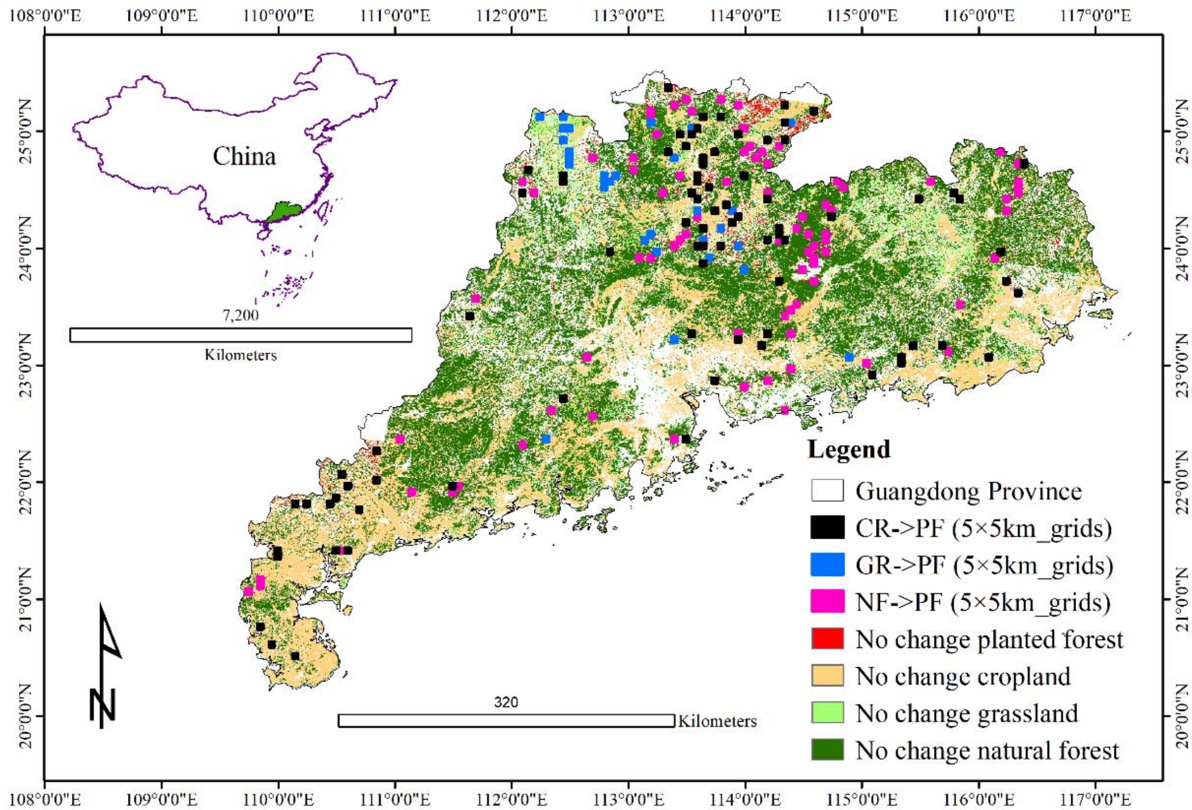

Figure 1. Location of the study area in Guangdong Province, southern China. Distribution of the areas with no change in land cover type, including planted forest (PF), cropland (CR), grassland (GR), and natural forest (NF) from 2000 to 2010 and sample grids (5 × 5 km). The black, blue, and purple boxes indicate the functional sample grid cells for converting cropland, grassland, and natural forests to planted forests, respectively.

Table 1. Remote sensing data used to extract biophysical and climate variables.

Dataset	Variables	Resolution	Time	Reference
MYD11A2	LST	1 km/8 days	2002–2010	(Wan, 2008)
MCD43B3	Albedo	1 km/8 days	2000–2010	(Schaaf et al., 2002)
MOD16A2	ET	1 km/8 days	2000–2010	(Mu et al., 2011)
MCD18A1	Downward shortwave flux	1 km/3 hours	2001-2010	(Wang et al., 2020)
LW_modis	Downward longwave flux	1 km/daily	2000-2010	(Cheng et al. 2017)

2.2. Estimating biophysical effects of hypothetical afforestation on surface temperature

To understand the biophysical effects of afforestation on LST between 2000 and 2010 in Guangdong Province, we adopted a space-for-time substitution method (Zhao and Jackson, 2014) to identify regions representing hypothetical afforestation and different conversion types. We then used the energy balance model and IBM theory to quantify the afforestation impacts on the LST.

2.2.1. Space-for-time method

The space-for-time method assumes that the adjacent pixels of PF and other land cover types have the same background climate. Hence, the local surface temperature differences are primarily driven by the land cover changes (Zhao and Jackson, 2014). Here the hypothetical afforestation refers to the forest change that has yet to happen in reality. By comparing the differences between adjacent pixel pairs of the PF and other land cover types, we can estimate the impacts of hypothetical afforestation in this area.

We first created 5 × 5 km grids across the entire study area and sampled those including NF, CR, GR, and PF that have not changed from 2000 to 2010.To identify proper grids representing the conversions from no change NF, CR or GR to the hypothetical PF, we then selected them based on the 1km land cover data from Section 2.1 following the rule: the cover of PF ≥ 5% and the cover of NF or open land (CR or GR) ≥ 80% (Figure 1). Within each selected grid, we adopted a window searching method (Zhao and Jackson, 2014) to identify the hypothetical changes by pairing adjacent pixels of PF and other types (NF, CR, and GR).

To assess the impacts of hypothetical afforestation on the local climatic and biophysical parameters, we calculated the multi-year mean values of LST, albedo, air temperature, and downward longwave and shortwave fluxes in the selected 5km grids. Then, for each conversion type, the afforestation induced changes were estimated by calculating the differences of these variables between the no change PF and the other types (NF, CR, or GR). Taking albedo as an example, the afforestation-induced albedo change (Δα) can be calculated as follows (Student's *t*-test: confidence interval (CI) is estimated by *t*-test at 95%, $p < 0.05$):

$$\Delta\alpha = \alpha_{PF} - \alpha_i, \quad (1)$$

where α_{PF} is the albedo of the PF after afforestation, α_i is the albedo of the CR, GR, or NF before afforestation, and *i* represents the CR, GR or NF. The differences in other biophysical and climate variables between PF and other types (NF, CR, and GR) were estimated in a similar fashion.

2.2.2. Modeling LST change due to hypothetical afforestation using the energy balance model and the IBM theory

The IBM theory assumes that the impacts of different land cover types on the LST are caused by local surface longwave radiative and energy redistribution induced by the aerodynamic resistance and Bowen ratio (Bright et al., 2017; Lee et al., 2011). The energy redistribution factor (*f*) reflects the surface energy balance of vegetation structure and physiology. Higher *f* values indicate that a vegetation ecosystem is more efficient at dissipating surface energy through intrinsic biogeophysical properties (Chen and Dirmeyer, 2016; Lee et al., 2011). The theory also assumes no differences in the low-atmosphere temperature between forest and open land (Winckler et al., 2017). The IBM theory is originated from the surface energy balance equation defined using Eq. (2) (Lee et al., 2011):

$$SW_{net} + LW_{\downarrow} - \sigma T_s^4 = R_n = H + LE + G, \quad (2)$$

where SW_{net} is the net surface shortwave radiation (W m^{-2}), $LW_{\downarrow}$ is the incoming longwave radiation (W m^{-2}), σ is the Stephan-Boltzmann constant (W m^{-2}K^{-4}), T_s is the surface temperature (K), R_n is the net radiation, H is the sensible heat flux, LE is the latent heat flux and G is the soil heat flux (W m^{-2}). Lee et al. (2011) pointed out that H and LE act as essential factors controlling the surface temperature (T_s) in the surface energy balance equation, so T_s can be estimated using Eqs. (3-5):

$$T_s = \frac{\lambda_0}{1+f}(R_n^* - G) + T_a, \quad (3)$$

$$R_n^* = SW_{net} + LW_{\downarrow} - \sigma T_a^4, \quad (4)$$

$$SW_{net} = (1-\alpha)SW_{\downarrow}, \quad (5)$$

where $\lambda_0 = 1/(4\sigma\varepsilon_s T_s^3)$ (K (W m^{-2})$^{-1}$) is the monthly mean temperature sensitivity of the longwave radiation feedback (ε_s is the monthly mean surface emissivity, $\varepsilon_s = 0.983$ for cropland and grassland, $\varepsilon_s = 0.989$ for forest (Caselles et al., 2011), T_a is the monthly mean air temperature (K), $SW_{\downarrow}$ is the incoming shortwave radiation (W m^{-2}), and R_n^* is the monthly apparent net radiation). G is the monthly mean soil heat flux, which is estimated as $G = 0.14(T_{a,n} - T_{a,n-1})$ (n represents month as 1, 2, …, 12) following Fischer et al. (2021). It is used for the calculation of the reference evapotranspiration of reference surfaces based on Penmann-Monteith equations and can be recognized. Then, we then modified Eq. (3) to estimate *f* from T_s, T_a, R_n^*, and G:

$$f = \frac{\lambda_0}{T_s - T_a}(R_n^* - G) - 1, \quad (6)$$

where T_s is the observed monthly surface temperature (K). Two equal values between T_s and T_a are invalid.

According to the IBM theory and the energy balance model based on Eqs. (2–5), several individual biophysical forcings induced by LULCC, including albedo, roughness, and ET, can affect the surface temperature changes (T_s). Thus, the total change in the modeled surface temperature (ΔT_{s_m}) due to afforestation can be separated into three sections, including the changes in the energy redistribution factor (Δf), radiative forcing (ΔR_n^*), and soil heat flux (ΔG), using the following equations (Bright et al., 2017):

$$\Delta R_n^* = \Delta SW_{\downarrow} = -SW_{\downarrow} \times \Delta\alpha, \quad (7)$$

$$\Delta T_{s\_m} = \frac{\lambda_0}{(1+f)}\Delta R_n^* + \frac{-\lambda_0}{(1+f)}\Delta G + \frac{-\lambda_0}{(1+f)^2}(R_n^* - G)\Delta f, \quad (8)$$

where λ_0, *f*, R_n^*, and G represent the variables for the CR, GR, and NF before afforestation. To address the differences in the variables between PF and open land (CR and GR), the variables in Eq. (8) were modified based on Eqs. (1) and (7) but excluded the atmospheric feedback as follows:

$$\Delta T_{s\_m} = \Delta T_{s\_\alpha} + \Delta T_{s\_G} + \Delta T_{s\_f}, \quad (9)$$

$$\Delta T_{s\_\alpha} = \frac{\lambda_i}{(1+f_i)}(-SW_{\downarrow i} \times (\alpha_{PF} - \alpha_i)), \quad (10)$$

$$\Delta T_{s\_G} = \frac{-\lambda_{0_i}}{(1+f_i)}(G_{PF} - G_i), (11)$$

$$\Delta T_{s\_f} = \frac{-\lambda_i}{(1+f_i)^2}(R_{n_i}^* - G_i)(f_{PF} - f_i), (12)$$

where ΔG and Δf are the differences in the multiyear monthly mean soil heat flux and energy redistribution factor (*f*) between the PF and other land cover types (CR, GR, and NF) from 2000 to 2010, similar to Δα in Eq. (1); while ΔT_{s_m} is the difference in the modeled surface temperature between the PF and other land cover types. This results from the joint contributions of the three parts in response to the temperature change caused by the forest change in Eq. (9). Specifically, ΔT_{s_α} represents the impact of the surface radiative forcing and albedo change on surface temperature; ΔT_{s_G} is the impact of the soil heat flux diffusion on surface temperature; ΔT_{s_f} is the impact of the turbulent energy redistribution on surface temperature. Then, the modeled surface temperate change (ΔT_{s_m}) was estimated using Eqs. (9–12). Positive ΔT_{s_m} values represent a warming effect due to afforestation, while negative values indicate cooling.

2.3. Comparing modeled and observed LST changes induced by afforestation

Then, we estimated ΔT_s using only MODIS data as the observed LST change (ΔT_{s_o}) caused by the hypothetical afforestation as a reference. The ΔT_{s_o} was obtained by comparing the T_s values of the PF and other land cover types following Eq. (1). We compared the afforestation-induced LST changes estimated with the two types of methods (ΔT_{s_m} and ΔT_{s_o}) and examined their linear relationships. We also assessed the relationships between ΔT_{s_m} and ΔT_{s_f}, ΔT_{s_α}, and ΔT_{s_G} using the monthly and seasonal values for the PF, NF, and open land via linear regression.

2.4. Identifying radiative and non-radiative effects of afforestation

The contributions of the radiative and non-radiative effects of afforestation to the ΔT_s were quantified and analyzed using the non-radiative forcing index (NRFI) (Bright et al., 2017):

$$\text{NRFI}\ (\%) = \frac{|\Delta T_{s\_f}| + |\Delta T_{s\_G}|}{|\Delta T_{s\_\alpha}| + |\Delta T_{s\_f}| + |\Delta T_{s\_G}|} \times 100, (13)$$

where ΔT_{s_α} is the albedo-driven LST change and represents the radiative effects of the afforestation-induced PF change; ΔT_{s_G} and ΔT_{s_f} refer to the G- and f-driven LST changes, respectively, and represent the non-radiative effects. A larger NRFI value indicates stronger non-radiative effects due to afforestation.

3. Results

3.1. Afforestation impacts on surface biophysical parameters and land surface fluxes

To evaluate the impacts of hypothetical afforestation on LST, 83, 30, and 84 5×5 km grids were sampled to represent the three conversion types, CR to PF, GR to PF, and NF to PF, respectively (Figure 1). For each conversion type, we calculated the Δf, Δα, ΔET, ΔR_n^*, and ΔG based on the no change PF and the CR, GR, and NF pixels between 2000 and 2010. The student's *t*-test revealed significant changes ($p < 0.05$) in the f, albedo (α), net radiation (R_n^*), and G for all three conversion types. We also reported the monthly mean values of Δf, $\Delta\alpha$, ΔET, ΔR_n^*, and ΔG induced by afforestation with their 95th percentiles (Figure 2).

The energy redistribution factor *f* generally increased after afforestation ($\Delta f > 0$), except for the afforestation on GR in summer and autumn and NF in autumn (Figure 2a). It can be observed across all seasons that the increases of *f* outweighed the decreases. Specifically, we found that the values of *f* after afforestation on CR showed a decreasing trend of 91.7% from spring to winter. The afforestation on GR in spring and winter also had positive Δf values. For afforestation on NF, Δf was positive (0.52) in summer, but became negative (−0.41) in autumn. Moreover, at the lower latitudes in Guangdong Province, the Δf values between PF and open land (CR/GR) were slightly higher than those between PF and NF (Figure S1). For CR, afforestation at the mid-high latitudes in Guangdong Province decreased *f* in spring, while this decrease in *f* mainly occurred in winter for NF (Figure S1).

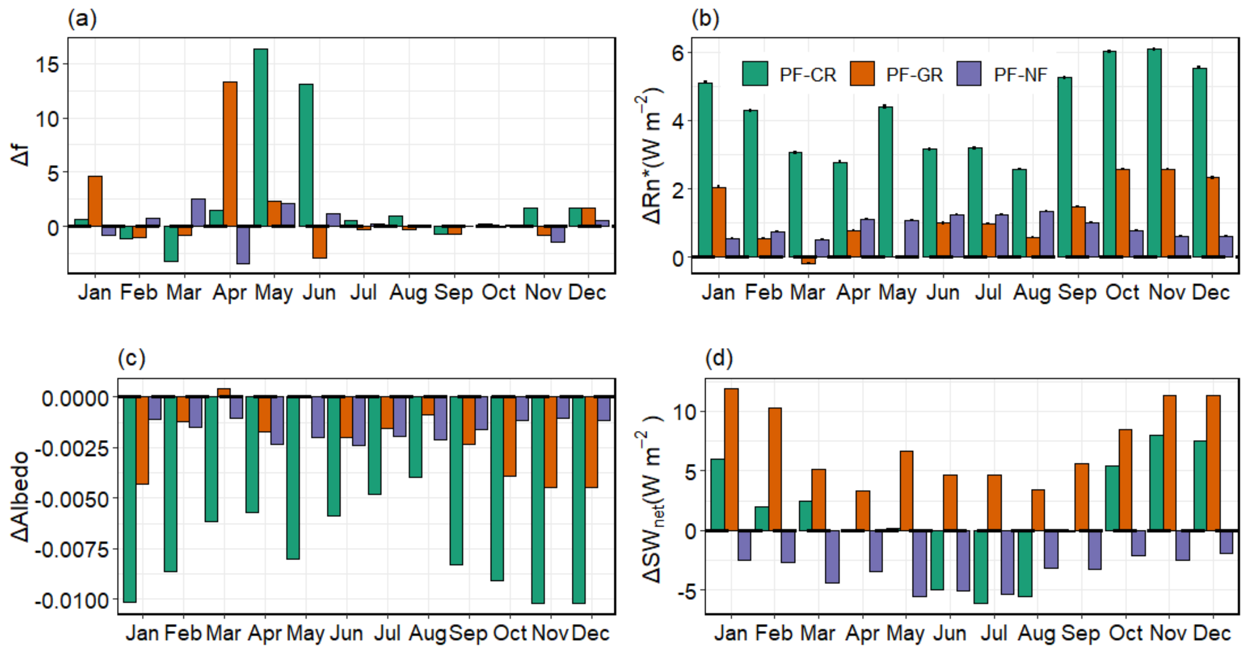

Figure 2. Monthly differences in the (a) energy redistribution factor *f* (Δf), (b) R_n^* (ΔR_n^*), (c)albedo ($\Delta\alpha$), and (d) SW_{net} (ΔSW_{net}) between the no change PF and CR, GR, and NF from 2000 to 2010 in Guangdong Province, China. Each bar's vertical lines represent the 95% confidence intervals estimated using the Student's *t*-test.

The annual variations in albedo were generally small and sometimes negligible. The highest and lowest negative $\Delta\alpha$ values occurred when converting NF and CR to PF, respectively (Figure 2c). Spatial and temporal variations in $\Delta\alpha$ existed for all three conversion types. We found a considerable decrease at the higher latitudes in Guangdong Province, except in summer. While a minor reduction was observed on the lower margins between the PF and CR, except for a more significant decrease in spring (21°N). A more significant reduction in $\Delta\alpha$ occurred at the mid-latitudes between PF and GR, and at the low latitudes between PF and NF (Figure S1). Except for the more significant decrease in summer (21°30’N), albedo had little effect at the lower latitudes. For converting open land to PF, $\Delta\alpha$ had the lowest value in winter.

Moreover, PF was less sensitive than GR to strong seasonal fluctuations in G, especially in summer and spring (Figure S2a). Those that were less sensitive than CR occurred in the winter and autumn; and those that were more sensitive than NF were found in the spring, summer, and autumn. We also found a negative relationship between the monthly G and albedo due to afforestation on GR (Figure S3a), yet linear relationships were not found between the monthly mean ΔG and ΔSW_{net} (Figure S3b). Additionally, for all conversion types, ΔSW_{net} had an overall downward trend from winter to summer and an upward trend from summer to winter (Figure 2d). The highest ΔSW_{net} value occurred when converting GR to PF.

Interestingly, consistent negative ΔET values were found among all conversion types throughout the year (Figure S2b). The ΔET values were the lowest when converting CR to PF and the highest when converting NF to PF. Yet the seasonal variations of ΔET were not obvious. Moreover, the relationship between ΔET and Δf was less pronounced (Figure S3c).

3.2. Impacts of afforestation on surface temperature

We then calculated and compared the mean values of the modeled ΔT_{s_m} driven by the energy redistribution factor (T_{s_f}), albedo (T_{s_α}), and soil heat flux change (T_{s_G}), as well as the observed T_{s_o} (Figures 3 and S4). For the modeled T_s changes, afforestation mainly had a net warming effects on NF, with annual ΔT_{s_m} values of 0.34±0.48 K. In contrast, a net cooling effect was found on CR (−0.17±0.87 K) and on GR (−0.02±0. 19 K). The spatial patterns of the ΔT_{s_m} also vary across all three-conversion types. Converting CR to PF could lead to warming in northern and southwestern Guangdong, but cooling in the south (Figures 4a and S4), while afforestation on NF resulted in warming across all latitudes. A cooling effect occurred for restoring GR to PF in northern Guangdong.

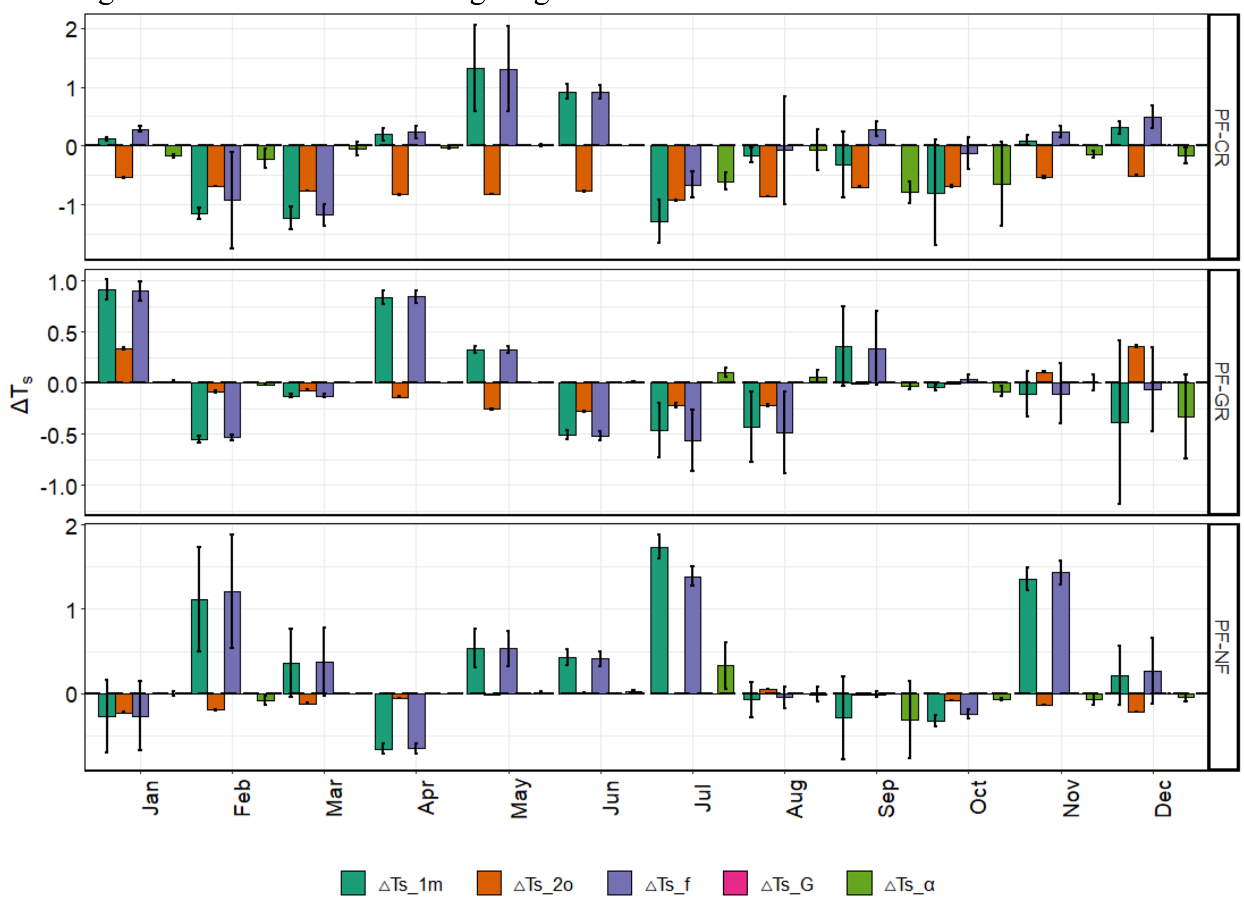

Figure 3. Monthly mean values of the modeled T_s change (ΔT_{s_m}), the observed T_s change (ΔT_{s_o}), the T_s change driven by the energy redistribution factor change (ΔT_{s_f}), the T_s change driven by the albedo change (ΔT_{s_α}), and the T_s change driven by the soil heat flux change (ΔT_{s_G}) for all three conversion types. Each bar's vertical lines represent the 95% confidence interval estimated using the Student's *t*-test.

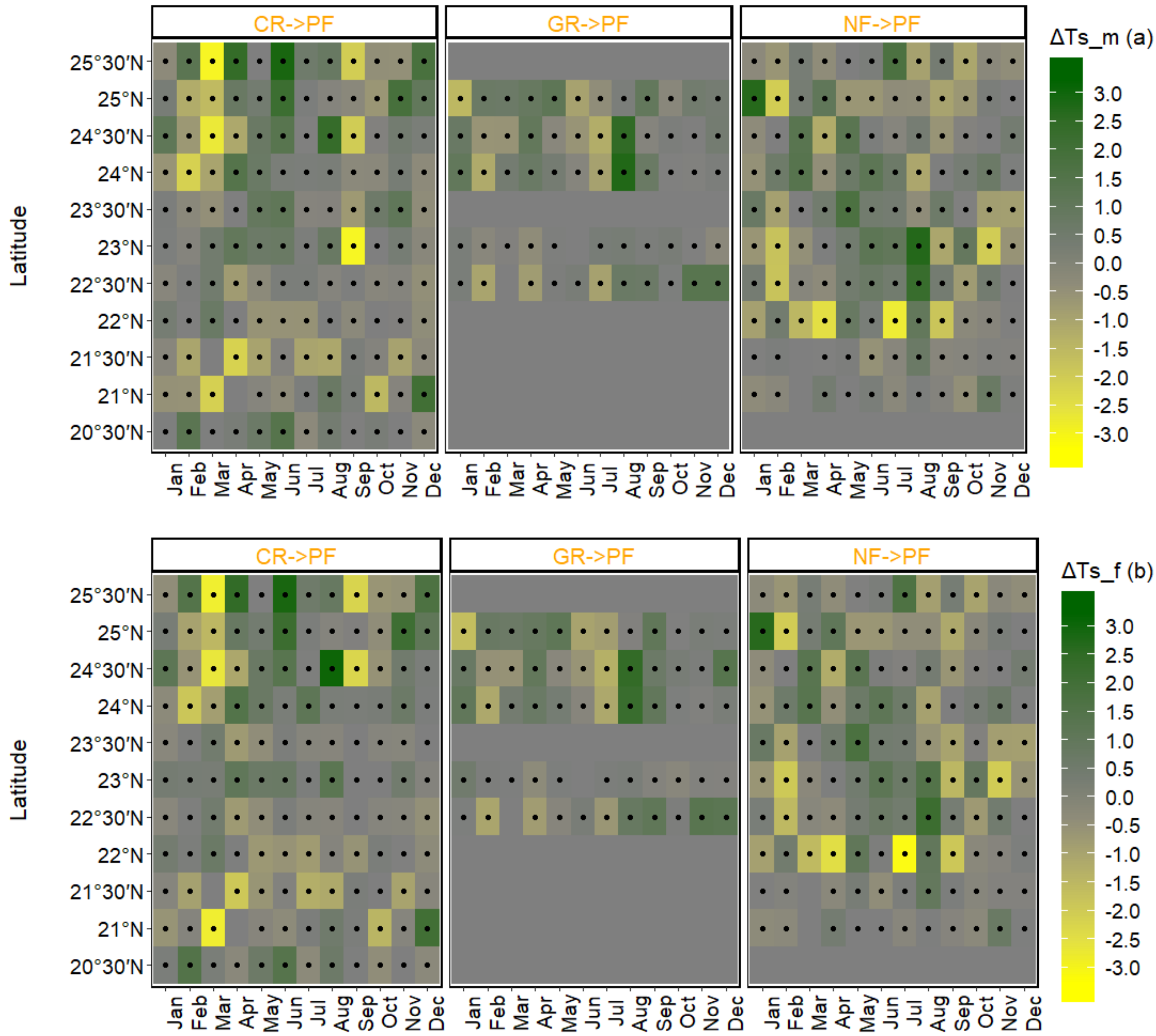

Figure 4. Monthly and latitudinal mean values of the modeled T_s change (ΔT_{s_m}, a) and the T_s change driven by the energy redistribution factor change (ΔT_{s_f}, b) for all three conversion types. The black dots represent the 95% significance level using the Student's *t*-test.

Noticeable differences were found between the ΔT_{s_m} and ΔT_{s_o} induced by afforestation, particularly on NF. For the observed ΔT_{s_o}, afforestation caused a net cooling effect for all conversion types (Figure 3), with the strongest on CR (−0.72±0.007 K), followed by that on NF (−0.087±0.002 K), and GR (−0.043±0.008 K). The monthly trends of ΔT_{s_m} and ΔT_{s_o} were also inconsistent in general (Figure 3). For example, we found a warming effect in the warm seasons and a cooling effect in the cold seasons due to afforestation on CR according to the ΔT_{s_m}. Yet, the observed T_s change (ΔT_{s_o}) suggested consistent cooling effects for all conversion types during warm seasons.

The modeled T_s change driven by $f\,(\Delta T_{s\_f})$ led to warming effects of 0.066±0.71 K, 0.001±0.17 K and 0.36±0.42 K when converting CR, GR, and NF to PF, respectively (Figures 3 and S4). The annual, monthly, and latitudinal ΔT_{s_f} were more spatially and temporally consistent with the ΔT_{s_m} than with the T_s changes driven by albedo (ΔT_{s_α}) and G (ΔT_{s_G}; Figures S4–S7, 3–5). The contributions of albedo and the soil heat flux to the modeled T_s change were also relatively small and negligible among all conversion types (Figures S4–S6, 3). Generally, the radiative process driven by the albedo change made small or negligible contributions to the modeled T_s change (Figures S6–S7). Whereas, the non-radiative process associated with the change in f as one of the primary partition variables dominates the modeled T_s change based on the strong linear relationship between ΔT_{s_f} and ΔT_{s_m} (Figure 5). Among these, the contributions of afforestation on NF were an exception because of a slight albedo effect (Figure S7).

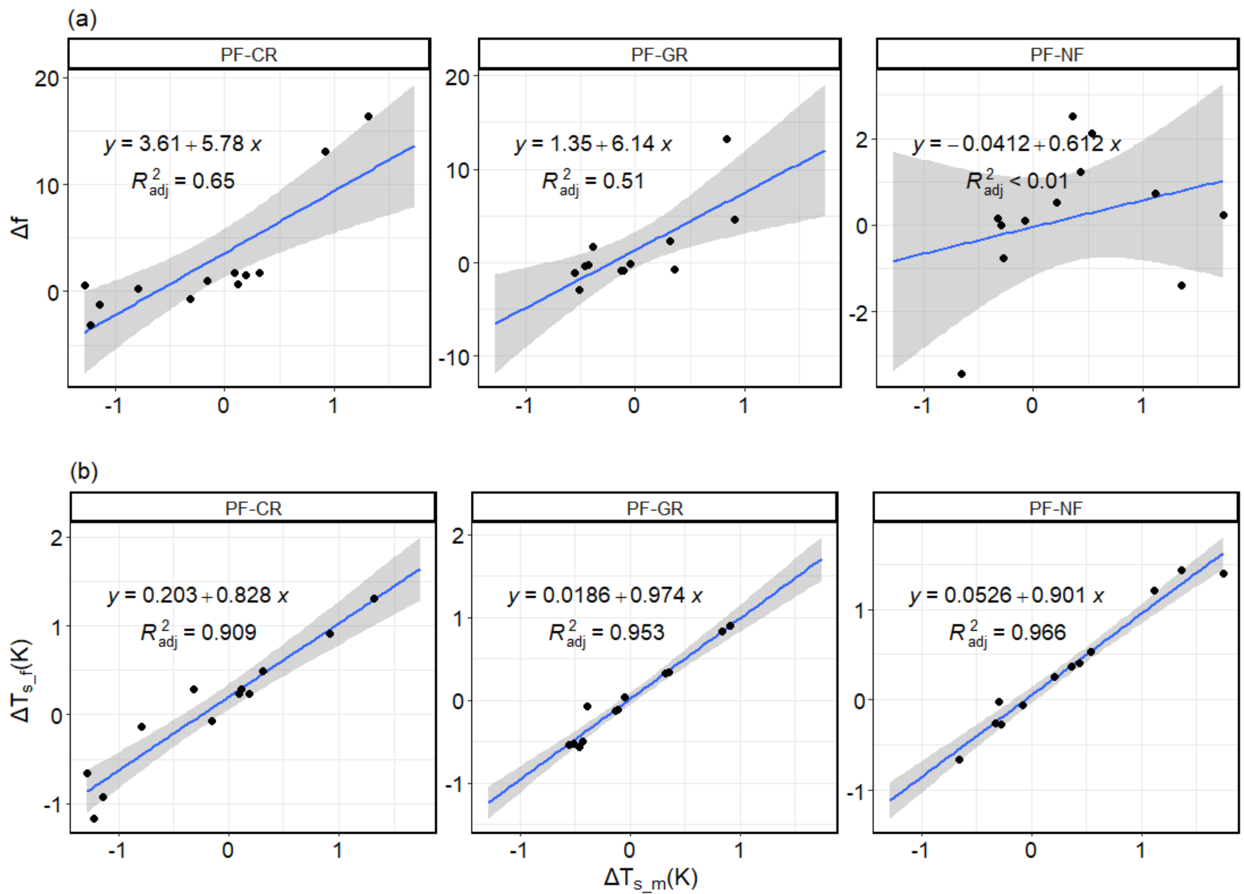

Figure 5. The relationships between the monthly values of ΔT_{s_m} and Δf (a), ΔT_{s_m} and ΔT_{s_f} (b) for the three conversion types. The blue lines are the linear regression lines. The gray solid line indicates the 95% confidence intervals (CI lines) and the shaded confidence area for the predictions.

3.3. Contributions of radiative and non-radiative effects of afforestation to surface temperature change

Afforestation had a warming effect of 0.143±0.43 K through the non-radiative processes and a cooling effect of −0.096±0.19 K via the radiative processes in Guangdong Province. The annual average of NRFI values were about 64.5%±0.79%, 80.2%±0.72%, and 75.3%±0.26% for converting CR, GR, and NF to PF, respectively (Figure 6). This indicates that the non-radiative processes contribute more than radiative processes to the T_s change in our study area. The differences in the NRFI values of the conversion types exist across months and latitudes. For the afforestation of NF, GR, and CR, the largest NRFI values were 94.7%±0.14% in March, 99.99%±0.002% in May, and 93.7%±0.32% in June; while the smallest NRFI values were 8.9%±0.08% in September, 33.0%±0.96% in October, and 19.1%±0.66% in October, respectively. Most of the monthly average NRFI values were above 73%±0.59%. The northern part of Guangdong experienced stronger non-radiative effects due to afforestation than the other regions for all conversion types, particularly for afforestation of GR (Figure S8).

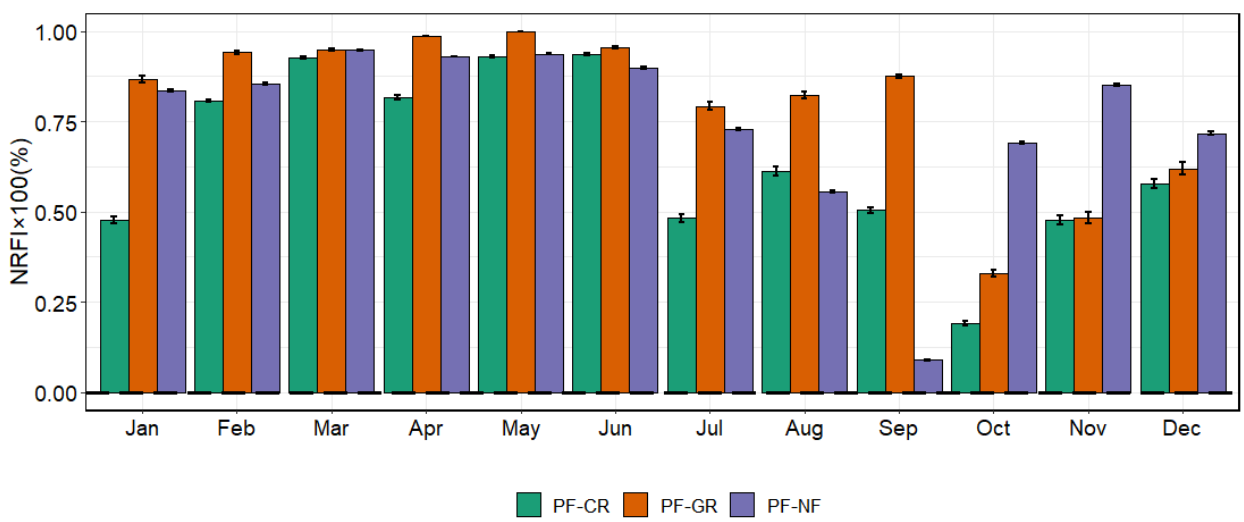

Figure 6. Monthly values of the non-radiative forcing index (NRFI) for the three conversion types. Each bar's vertical lines represent the 95% confidence interval estimated using the Student's *t*-test.

4. Discussions

In this study, we found the impact of the hypothetical afforestation from 2000 to 2010 in Guangdong Province, southern China on the modeled land surface temperature using the surface energy balance model and IBM theory showed a slight warming effect. Afforestation on open land (CR and GR) produced an overall cooling effect from north to south, which is consistent with the results of previous studies (Alkama and Cescatti, 2016; Li et al., 2015; Peng et al., 2014; Prevedello et al., 2019). Yet, the effects of afforestation on the land surface temperature when converting NF to PF obtained using modeled and observed results were contradictory, which can be explained from several perspectives.

Converting natural forests to planted forests can have a warming effect on LST because the conifer forests have dark leaves and low albedo, thus can absorb more sunlight than underground, which is different from that of broadleaved forests (Popkin, 2019; Shen et al., 2019b). This could also explain the finding that the warming impact occurred in the warm seasons. Unlike the contradictory results mentioned above, converting CR and GR to PF resulted in cooling effects based on both the modeled and observed T_s change, which is consistent with the results of previous studies (Bright et al., 2017; Ge et al., 2019), although the effect displayed by the observed results was stronger. Compared to grasslands and croplands, forests have a higher capacity to transfer latent heat and sensible heat to the atmosphere (Jackson et al., 2008). The roughness and aerodynamic conductance of the forest canopy are significantly higher than that of herbaceous vegetation and crop, leading to the forest canopy being cooler than the grasslands and croplands (Houspanossian et al., 2013; Kelliher et al., 1993; Lee et al., 2011). Moreover, the decrease in the shortwave radiation after afforestation on grassland can contribute to the temperature decrease as well (Yang, 1999). The warming effect of converting cropland to forest, especially irrigated cropland, occurs in northern and southwestern Guangdong, which is consistent with the studies from Ge et al. (2019) and Kueppers et al. (2008).

In general, the biophysical mechanisms of the radiative and non-radiative processes can provide plausible explanations for the modeled T_s change results due to afforestation across Guangdong Province. The combined effects of these processes drive the spatiotemporal variations in the surface temperature change due to afforestation. Afforestation can lead to warming due to a lower albedo of forests than open land; however, albedo does not play a dominant role in either method (Anderson et al., 2011; Betts, 2000). In addition, forests can lead to evaporative cooling. However, this was not revealed by the observed results because satellite observations do not consider the effects of the energy balance process. This suggests that the IBM-based method adopted in this study can provide more insights for investigating the impacts of afforestation on the local environment. It is also reasonable that the ET change did not dominate the afforestation effects since the higher evaporation loss from planted forests may lead to problems with water management and the local climate (Nosetto et al., 2005). Additionally, the change in G had little effect on the overall results, which is consistent with Ge et al. (2019). Forests are typically less sensitive to G than herbaceous species (Yang, 1999). Under a high solar radiation load, the land cover types with lower vegetation cover, such as rain-fed cropland and grassland, have higher G values. The heat fluxes of these categories are nearly zero and negligible.

The non-radiative effects of afforestation, particularly the Δf, are the major contributors to the warming effect in open land (cropland and grassland), and they explain more than 73% of the warming (i.e., the change in T_s) (Figures 5–6). The spatial and seasonal variations in the Δf were also consistent with previous studies conducted on afforestation (Bright et al., 2017; Ge et al., 2019; Lee et al., 2011). However, the aerodynamic resistance-based f value may overestimate the impacts of the non-radiative processes on the surface temperature (Liao et al., 2018; Rigden and Li, 2017). As for natural forests, we did not observe obvious effects of some of the spatial inconsistencies compared to the results of previous studies. These anomalies could be caused by the higher resolution data we used to describe the spatiotemporal distribution of the afforestation. More studies on high-resolution land cover type identification are required, such as different forest species, irrigated cropland and rain-fed cropland (Kueppers et al., 2008; Prevedello et al., 2019).

Our study also suggested that the IBM-based method is more indicative for studying the biophysical effects of afforestation at a regional scale (Bright et al., 2017; Wang et al., 2020). Compared to Ge et al. (2019), we adopted different land cover data and parameters for the energy balance model, which could lead to different results. Studies of afforestation in the arid regions of northern China also found opposite results using different approaches, such as regional climate models and site observations based on the IBM theory (Wang et al., 2019; Wang et al., 2018). It has been concluded that the former (Wang et al., 2019) considered the biophysical effects of afforestation based on the regional climate model and the effects of atmospheric feedback. Although we did not use climate models and concluded that the local climate feedbacks were consistent, our study thoroughly analyzed the biophysical impacts of afforestation on different land cover types using fine-identification data for afforestation as inputs to the model.

The results we obtained using the physical-based method for afforestation of open land were consistent with those from satellite observations-based results and Ge et al. (2019), in which afforestation led to cooling. Yet, the total warning effect was inconsistent with those derived from the satellite observations in this study and with the findings of previous studies, which suggested a total cooling effect due to afforestation of open land and natural forest (Peng et al., 2014; Shen et al., 2019b). Several factors could contribute to these differences. Firstly, our analyses were conducted based on hypothetical afforestation using the space-for-time method. Though this strategy has been commonly adopted (Chapman, 2020; Chilukoti and Xue, 2020; Ge et al., 2019; Peng et al., 2014; Zhao and Jackson, 2014) and produced comparable results of LST trends with the actual forest changes (Li et al., 2016), using the hypothetical afforestation for analysis could still induce uncertainties in results because it is not exactly the actual forest cover change. Secondly, though the non-local effects of atmospheric feedbacks on afforestation are typically less significant at small scales (Lee et al., 2011) and thus ignored in this study, afforestation can indirectly affect the local temperature through feedbacks from the atmosphere (Devaraju et al., 2018; Li et al., 2020). Also, uncertainties could be introduced by the input datasets through the resampling methods and some hypothetical parameter values that have not been independently validated as well as errors that exist in surface temperature driven by three biophysical parameters. Future work could incorporate more accurate biophysical or climatic variables and detailed land cover types, such as specific tree species and crop types, for developing an enhanced understanding of afforestation impacts on the local environment. The satellite and biophysical parameters used in this energy balance model were restricted to non-overcast conditions, which could lead to an overestimation of the afforestation impacts on the surface temperature (Bright et al., 2017; Ge et al., 2019). The temperature effect of radiation difference caused by topography is also negligible (Lee et al., 2013; Hao et al., 2021).

Forest changes can modify the thermal and hydrological cycles of local ecosystems through the radiative and non-radiative effects of biophysical processes, while the water resources, soil properties, and background climate affect the contributions of forests to climate (Anderson et al., 2011; Perugini et al., 2017). Further separation of the effects of the energy redistribution parameters such as the latent heat, sensible heat flux, and Bowen ratio on the temperature could provide more meaningful insights into the interactions between forest change and the local ecosystems. Furthermore, multi-source data such as high-resolution afforestation data and satellite observations, surface energy flux data, climate models, and *in situ* measurements can be integrated in the future to investigate the land-atmospheric interactions related to land cover changes (Perugini et al., 2017). Additionally, though afforestation is an important tool for mitigating climate change, restoring lost forest area and maintaining existing forests are critical for preventing further biophysical surface warming in local regions (Bright et al., 2017).

5. Conclusions

In this study, we integrated satellite data and a surface energy balance model to investigate the biophysical impacts of afforestation on the land surface temperature in Guangdong Province, southern China. This study proposes a framework for understanding the biophysical effects of forest changes due to afforestation on local surface temperature by integrating high-resolution land cover data and an energy balance model. Results from satellite observations and the physical-based model both suggested a cooling effect of afforestation on open land (CR and GR) across our study area. Nevertheless, we found that the annual warming impact of the afforestation of natural forest obtained using the modeled surface temperature change differed from the satellite observation-based results. The change in f dominates this modeled temperature result. In general, the non-radiative processes lead to warming, while the radiative processes lead to slight cooling. The most significant cooling and warming due to the non-radiative processes occurred over forests converted from open land and natural forest, respectively.

Identifying detailed land cover types and selecting appropriate types for afforestation should be improved in the practical evaluation of the temperature response and the mitigation of regional increases in temperature. Our methods and findings can provide guidance for designing rational afforestation plans in southern China and similar geographic areas.

Acknowledgments

- Our work was jointly funded or supported by the National Natural Science Foundation of China (32001251), Natural Science Foundation of Jiangsu Province (BK20200781), and the Priority Academic Program Development of Jiangsu Higher Education Institutions (PAPD).
- The authors also thank the Guangdong Provincial Center for Forest Resources Monitoring for providing field inventories. It is also the appropriate place to thank colleagues and other contributors.

Data Availability Statement

Biophysical and climatic data are available from MODIS products through public resources. The no change planted forests, natural forests, and open lands data in 2000-2010 can be found at https://doi.org/10.6084/m9.figshare.19982726.v3. The surface biophysical parameters and land surface fluxes data can be found at https://doi.org/10.6084/m9.figshare.20107175.v1. Data and grids used for modeling LST change due to hypothetical afforestation can be found at https://doi.org/10.6084/m9.figshare.20107973.v1. And the non-radiative forcing index (NRFI) and land surface temperature change data due to afforestation can be found at https://doi.org/10.6084/m9.figshare.20109944.v1. All R code used in data processing can be found at https://doi.org/10.6084/m9.figshare.20105423.v2.

References

Alkama, R., & Cescatti, A. (2016). Biophysical climate impacts of recent changes in global forest cover. Science, 351(6273), 600-604. https://doi.org/10.1126/science.aac8083

Anderson, R. G., Canadell, J. G., Randerson, J. T., Jackson, R. B., Hungate, B. A., Baldocchi, D. D., et al. (2011). Biophysical considerations in forestry for climate protection. Frontiers In Ecology And the Environment, 9(3), 174-182. https://doi.org/10.1890/090179

Betts, R. A. (2000). Offset of the potential carbon sink from boreal forestation by decreases in surface albedo. Nature, 408(6809), 187-190

Bonan, G. B. (2008). Forests and Climate Change Forcings, Feedbacks, and the Climate Benefits of Forests. Science, 320(5882), 1444-1449

Bright, R. M., Davin, E., O'Halloran, T., Pongratz, J., Zhao, K., & Cescatti, A. (2017). Local temperature response to land cover and management change driven by non-radiative processes. Nature Climate Change, 7(4), 296-302. https://doi.org/10.1038/nclimate3250

Brown, S., Lugo, A. E., & Chapman, J. D. (1986). Biomass of Tropical Tree Plantation and its implications for the global carbon budget. Candian Journal of Forest Research, 16, 390-394

Caselles, E., Abad, F. J., Valor, E., & Caselles, V. (2011). Automatic Generation of Land Surface Emissivity Maps. Climate Change-Research and Technology for Adaptation and Mitigation, 15.

Chapman, M., Walker, W. S., Cook - Patton, S. C., Ellis, P. W., Farina, M., Griscom, B. W., & Baccini, A. (2020). Large climate mitigation potential from adding trees to agricultural lands. Global Change Biology Bioenergy

Chen, J., Chen, J., Liao, A., Cao, X., Chen, L., Chen, X., et al. (2015). Global land cover mapping at 30m resolution: A POK-based operational approach. ISPRS Journal of Photogrammetry and Remote Sensing, 103, 7-27. https://doi.org/10.1016/j.isprsjprs.2014.09.002

Chen, L., & Dirmeyer, P. A. (2016). Adapting observationally based metrics of biogeophysical feedbacks from land cover/land use change to climate modeling. Environmental Research Letters, 11(3). https://doi.org/10.1088/1748-9326/11/3/034002

Chen, L., & Dirmeyer, P. A. (2020). Reconciling the disagreement between observed and simulated temperature responses to deforestation. Nature Communications, 11(1), 202. https://doi.org/10.1038/s41467-019-14017-0

Chilukoti, N., & Xue, Y. (2020). An assessment of potential climate impact during 1948–2010 using historical land use land cover change maps. International Journal of Climatology. https://doi.org/10.1002/joc.6621

Devaraju, N., de Noblet-Ducoudré, N., Quesada, B., & Bala, G. (2018). Quantifying the Relative Importance of Direct and Indirect Biophysical Effects of Deforestation on Surface Temperature and Teleconnections. Journal of Climate, 31(10), 3811-3829. https://doi.org/10.1175/jcli-d-17-0563.1

Duveiller, G., Hooker, J., & Cescatti, A. (2018). The mark of vegetation change on Earth's surface energy balance. Nature Communications, 9(1), 679. https://doi.org/10.1038/s41467-017-02810-8

Fischer, G., Nachtergaele, F.O., van Velthuizen, H.T., Chiozza, F., Franceschini, G., Henry, M., et al. (2021). Global Agro-Ecological Zones v4–Model documentation. Food & Agriculture Org.

Ge, J., Guo, W., Pitman, A. J., De Kauwe, M. G., Chen, X., & Fu, C. (2019). The Nonradiative Effect Dominates Local Surface Temperature Change Caused by Afforestation in China. Journal of Climate, 32(14), 4445-4471. https://doi.org/10.1175/JCLI-D-18-0772.1

Gelaro, R., McCarty, W., Suarez, M. J., Todling, R., Molod, A., Takacs, L., et al. (2017). The Modern-Era Retrospective Analysis for Research and Applications, Version 2 (MERRA-2). J Clim, Volume 30(Iss 13), 5419-5454. https://doi.org/10.1175/JCLI-D-16-0758.1

Hao, D., Bisht, G., Gu, Y., Lee, W. L., Liou, K. N., & Leung, L. R. (2021). A parameterization of sub-grid topographical effects on solar radiation in the E3SM Land Model (version 1.0): implementation and evaluation over the Tibetan Plateau. Geoscientific Model Development, 14(10), 6273-6289. https://doi.org/10.5194/gmd-14-6273-2021

He, T., Shao, Q., Cao, W., Huang, L., & Liu, L. (2015). Satellite-Observed Energy Budget Change of Deforestation in Northeastern China and its Climate Implications. Remote Sensing, 7(9), 11586-11601. https://doi.org/10.3390/rs70911586

Houspanossian, J., Nosetto, M., & Jobbagy, E. G. (2013). Radiation budget changes with dry forest clearing in temperate Argentina. Globe Change Biology, 19(4), 1211-1222. https://doi.org/10.1111/gcb.12121

Huang, B., Hu, X., Fuglstad, G. A., Zhou, X., Zhao, W., & Cherubini, F. (2020). Predominant regional biophysical cooling from recent land cover changes in Europe. Nature Communications, 11(1), 1-13. https://doi.org/10.1038/s41467-020-14890-0

Jackson, R. B., Randerson, J. T., Canadell, J. G., Anderson, R. G., Avissar, R., Baldocchi, D. D., et al. (2008). Protecting climate with forests. Environmental Research Letters, 3(4), 044006. https://doi.org/10.1088/1748-

9326/3/4/044006
Kelliher, F. M., Leuning, R., & Schulze, E. D. (1993). Evaporation and canopy characteristics of coniferous forests and grasslands. Oecologia, 95(2), 153-163. https://doi.org/10.1007/BF00323485
Kueppers, L. M., Snyder, M. A., Sloan, L. C., Cayan, D., Jin, J., Kanamaru, H., et al. (2008). Seasonal temperature responses to land-use change in the western United States. Global and Planetary Change, 60(3-4), 250-264. https://doi.org/10.1016/j.gloplacha.2007.03.005
Lee, X., Goulden, M. L., Hollinger, D. Y., Barr, A., Black, T. A., Bohrer, G., et al. (2011). Observed increase in local cooling effect of deforestation at higher latitudes. Nature, 479(7373), 384-387. https://doi.org/10.1038/nature10588
Lee, W. L., Liou, K. N., & Wang, C. C. (2013). Impact of 3-D topography on surface radiation budget over the Tibetan Plateau.Theoretical and applied climatology,113.1, 95-103. https://doi.org/10.1007/s00704-012-0767-y
Li, Y., Liu, Y., Bohrer, G., Cai, Y., Wilson, A., Hu, T., et al. (2022). Impacts of forest loss on local climate across the conterminous United States: Evidence from satellite time-series observations. Science of the Total Environment, 802, 149651. https://doi.org/10.1016/j.scitotenv.2021.149651
Li, Y., Piao, S. L., Chen, A. P., Ciais, P., & Li, L. Z. X. (2020). Local and teleconnected temperature effects of afforestation and vegetation greening in China. National Science Review, 7(5), 897-912. https://doi.org/10.1093/nsr/nwz132
Li, Y., Zhao, M., Mildrexler, D. J., Motesharrei, S., Mu, Q., Kalnay, E., et al. (2016). Potential and Actual impacts of deforestation and afforestation on land surface temperature. Journal of Geophysical Research: Atmospheres, 121(24), 14,372-314,386. https://doi.org/10.1002/2016jd024969
Li, Y., Zhao, M., Motesharrei, S., Mu, Q., Kalnay, E., & Li, S. (2015). Local cooling and warming effects of forests based on satellite observations. Nature Communications, 6, 6603. https://doi.org/10.1038/ncomms7603
Liao, W., Rigden, A. J., & Li, D. (2018). Attribution of Local Temperature Response to Deforestation. Journal of Geophysical Research: Biogeosciences, 123(5), 1572-1587. https://doi.org/10.1029/2018jg004401
Lund, H. G. (2006), Definitions of forest, deforestation, afforestation, and reforestation, Forest Information Services Gainesville, VA.
Luyssaert, S., Jammet, M., Stoy, P. C., Estel, S., Pongratz, J., Ceschia, E., et al. (2014). Land management and land-cover change have impacts of similar magnitude on surface temperature. Nature Climate Change, 4(5), 389-393. https://doi.org/10.1038/nclimate2196
Mahmood, R., Pielke Sr, R. A., Hubbard, K. G., Niyogi, D., Dirmeyer, P. A., McAlpine, C., & ... & Fall, S. (2014). Land cover changes and their biogeophysical effects on climate. International Journal of Climatology, 34(4), 929-953
Mu, Q. Z., Zhao, M. S., & Running, S. W. (2011). Improvements to a MODIS global terrestrial evapotranspiration algorithm. Remote Sensing of Environment, 115(8), 1781-1800. https://doi.org/10.1016/j.rse.2011.02.019
Nosetto, M. D., Jobbagy, E. G., & Paruelo, J. M. (2005). Land-use change and water losses: the case of grassland afforestation across a soil textural gradient in central Argentina. Global Change Biology, 11(7), 1101-1117. https://doi.org/10.1111/j.1365-2486.2005.00975.x
Novo-Fernández, A., Franks, S., Wehenkel, C., López-Serrano, P. M., Molinier, M., & López-Sánchez, C. A. (2018). Landsat time series analysis for temperate forest cover change detection in the Sierra Madre Occidental, Durango, Mexico. International Journal of Applied Earth Observation and Geoinformation, 73, 230-244. https://doi.org/10.1016/j.jag.2018.06.015
Peng, S. S., Piao, S., Zeng, Z., Ciais, P., Zhou, L., Li, L. Z., et al. (2014). Afforestation in China cools local land surface temperature. Proceedings of the National Academy of Sciences of the United States of America, 111(8), 2915-2919. https://doi.org/10.1073/pnas.1315126111
Perugini, L., Caporaso, L., Marconi, S., Cescatti, A., Quesada, B., de Noblet-Ducoudré, N., et al. (2017). Biophysical effects on temperature and precipitation due to land cover change. Environmental Research Letters, 12(5), 053002. https://doi.org/10.1088/1748-9326/aa6b3f
Popkin, G. (2019). How much can forest fight climate change? Trees are supposed to slow global warming, but growing evidence suggests they might not always be climate saviours. Nature, 565, 280-282
Prevedello, J. A., Winck, G. R., Weber, M. M., Nichols, E., & Sinervo, B. (2019). Impacts of forestation and deforestation on local temperature across the globe. Plos One, 14(3), e0213368. https://doi.org/10.1371/journal.pone.0213368
Rigden, A. J., & Li, D. (2017). Attribution of surface temperature anomalies induced by land use and land cover changes. Geophysical Research Letters, 44(13), 6814-6822. https://doi.org/10.1002/2017gl073811
Schaaf, C. B., Gao, F., Strahler, A. H., Lucht, W., Li, X., Tsang, T., & Lewis, P. (2002). First operational BRDF, albedo nadir reflectance products from MODIS. Remote Sensing of Environment, 83(1-2), 135-148

Senior, R. A., Hill, J. K., Gonzalez Del Pliego, P., Goode, L. K., & Edwards, D. P. (2017). A pantropical analysis of the impacts of forest degradation and conversion on local temperature. Ecology and Evolution, 7(19), 7897-7908. https://doi.org/10.1002/ece3.3262

Shen, W., He, J., Huang, C., & Li, M. (2020). Quantifying the Actual Impacts of Forest Cover Change on Surface Temperature in Guangdong, China. Remote Sensing, 12(15), 2354. https://doi.org/10.3390/rs12152354

Shen, W., Li, M., Huang, C., Tao, X., Li, S., & Wei, A. (2019a). Mapping Annual Forest Change Due to Afforestation in Guangdong Province of China Using Active and Passive Remote Sensing Data. Remote Sensing, 11(5), 490. https://doi.org/10.3390/rs11050490

Shen, W., Li, M., Huang, C., Tao, X., & Wei, A. (2018). Annual forest aboveground biomass changes mapped using ICESat/GLAS measurements, historical inventory data, and time-series optical and radar imagery for Guangdong province, China. Agricultural and Forest Meteorology, 259, 23-38. https://doi.org/10.1016/j.agrformet.2018.04.005

Shen, W. J., Li, M. S., Huang, C. Q., He, T., Tao, X., & Wei, A. S. (2019b). Local land surface temperature change induced by afforestation based on satellite observations in Guangdong plantation forests in China. Agricultural and Forest Meteorology, 276-277, 107641. https://doi.org/10.1016/j.agrformet.2019.107641

Tang, B., Zhao, X., & Zhao, W. (2018). Local Effects of Forests on Temperatures across Europe. Remote Sensing, 10(4), 529. https://doi.org/10.3390/rs10040529

Wan, Z. (2008). New refinements and validation of the MODIS Land-Surface Temperature/Emissivity products. Remote Sensing of Environment, 112(1), 59-74. https://doi.org/10.1016/j.rse.2006.06.026

Wang, L., Lee, X., Feng, D., Fu, C., Wei, Z., Yang, Y., et al. (2019). Impact of Large-Scale Afforestation on Surface Temperature: A Case Study in the Kubuqi Desert, Inner Mongolia Based on the WRF Model. Forests, 10(5), 368. https://doi.org/10.3390/f10050368

Wang, L., Lee, X., Schultz, N., Chen, S., Wei, Z., Fu, C., et al. (2018). Response of Surface Temperature to Afforestation in the Kubuqi Desert, Inner Mongolia. Journal of Geophysical Research: Atmospheres, 123(2), 948-964. https://doi.org/10.1002/2017jd027522

Wang, L., Tian, F., Wang, X., Yang, Y., & Wei, Z. (2020). Attribution of the land surface temperature response to land-use conversions from bare land. Global and Planetary Change, 193, 103268. https://doi.org/10.1016/j.gloplacha.2020.103268

Wickham, J. D., Wade, T. G., & Riitters, K. H. (2013). Empirical analysis of the influence of forest extent on annual and seasonal surface temperatures for the continental United States. Global Ecology And Biogeography, 22(5), 620-629. https://doi.org/10.1111/geb.12013

Winckler, J., Reick, C. H., & Pongratz, J. (2017). Robust Identification of Local Biogeophysical Effects of Land-Cover Change in a Global Climate Model. Journal of Climate, 30(3), 1159-1176. https://doi.org/10.1175/jcli-d-16-0067.1

Yang, Z. L., Dai, Y., Dickinson, R. E., & Shuttleworth, W. J. (1999). Sensitivity of ground heat flux to vegetation cover fraction and leaf area index. Journal of Geophysical Research: Atmospheres, 104(D16), 19505-19514

Yu, L., Zhang, S., Tang, J., Liu, T., Bu, K., Yan, F., et al. (2015). The effect of deforestation on the regional temperature in Northeastern China. Theoretical and Applied Climatology, 120(3-4), 761-771. https://doi.org/10.1007/s00704-014-1186-z

Zhao, K., & Jackson, R. (2014). Biophysical forcings of land-use changes from potential forestry activities in North America. Ecological Monographs, 84(2), 329-353

Figure 1.

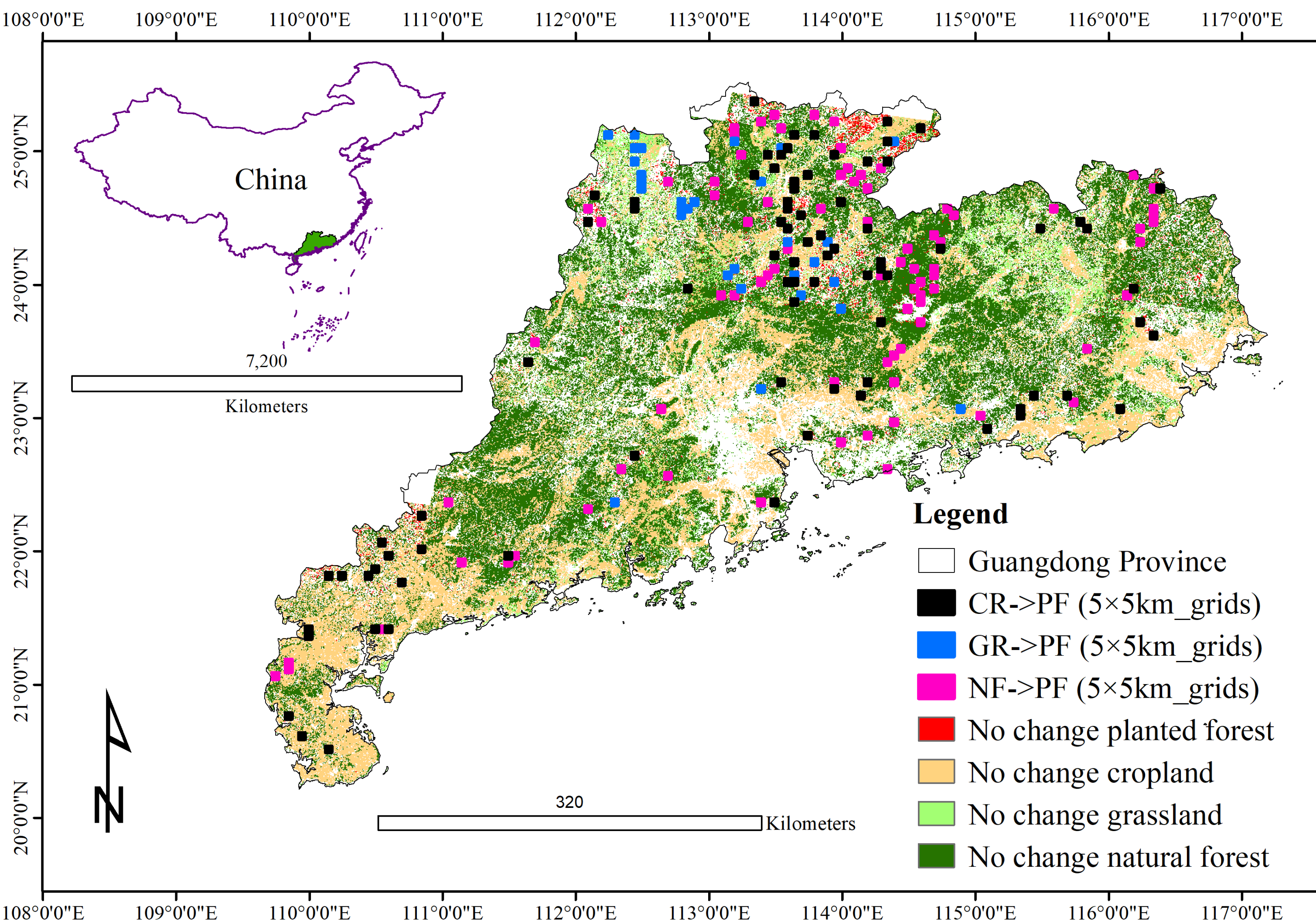
108°0'0"E
109°0'0"E
110°0'0"E
111°0'0"E
112°0'0"E
113°0'0"E
114°0'0"E
115°0'0"E
116°0'0"E
117°0'0"E
25°0'0"N
24°0'0"N
23°0'0"N
22°0'0"N
21°0'0"N
20°0'0"N
China
7,200
Kilometers
320
Kilometers
N
Legend
Guangdong Province
CR->PF (5×5km_grids)
GR->PF (5×5km_grids)
NF->PF (5×5km_grids)
No change planted forest
No change cropland
No change grassland
No change natural forest

Figure 2.

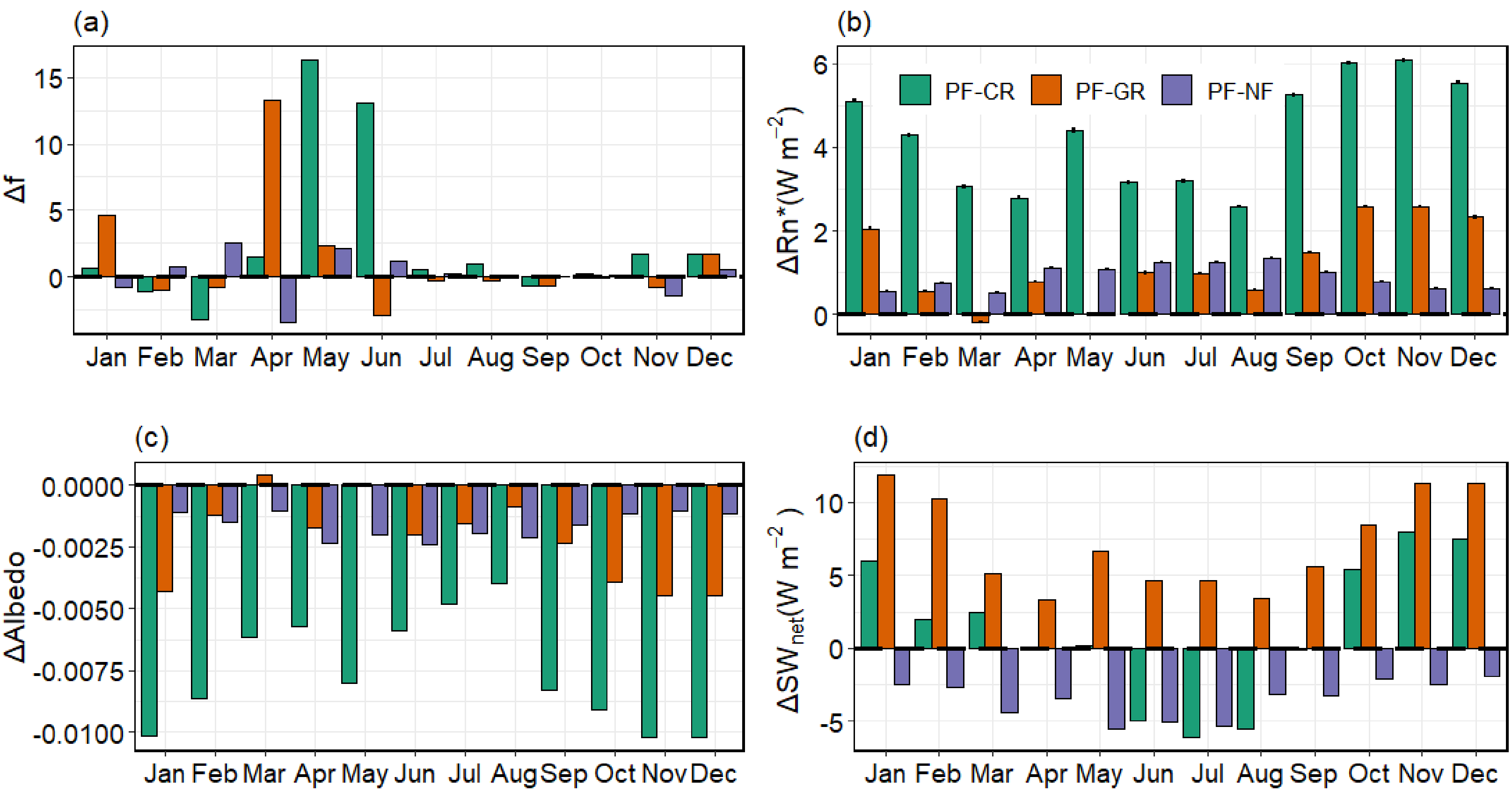

(a)
Δf
15
10
5
0
Jan Feb Mar Apr May Jun Jul Aug Sep Oct Nov Dec
(b)
PF-CR
PF-GR
PF-NF
ΔRn*(W m^-2)
6
4
2
0
Jan Feb Mar Apr May Jun Jul Aug Sep Oct Nov Dec
(c)
ΔAlbedo
0.0000
-0.0025
-0.0050
-0.0075
-0.0100
Jan Feb Mar Apr May Jun Jul Aug Sep Oct Nov Dec
(d)
ΔSW_net(W m^-2)
10
5
0
-5
Jan Feb Mar Apr May Jun Jul Aug Sep Oct Nov Dec

Figure 3.

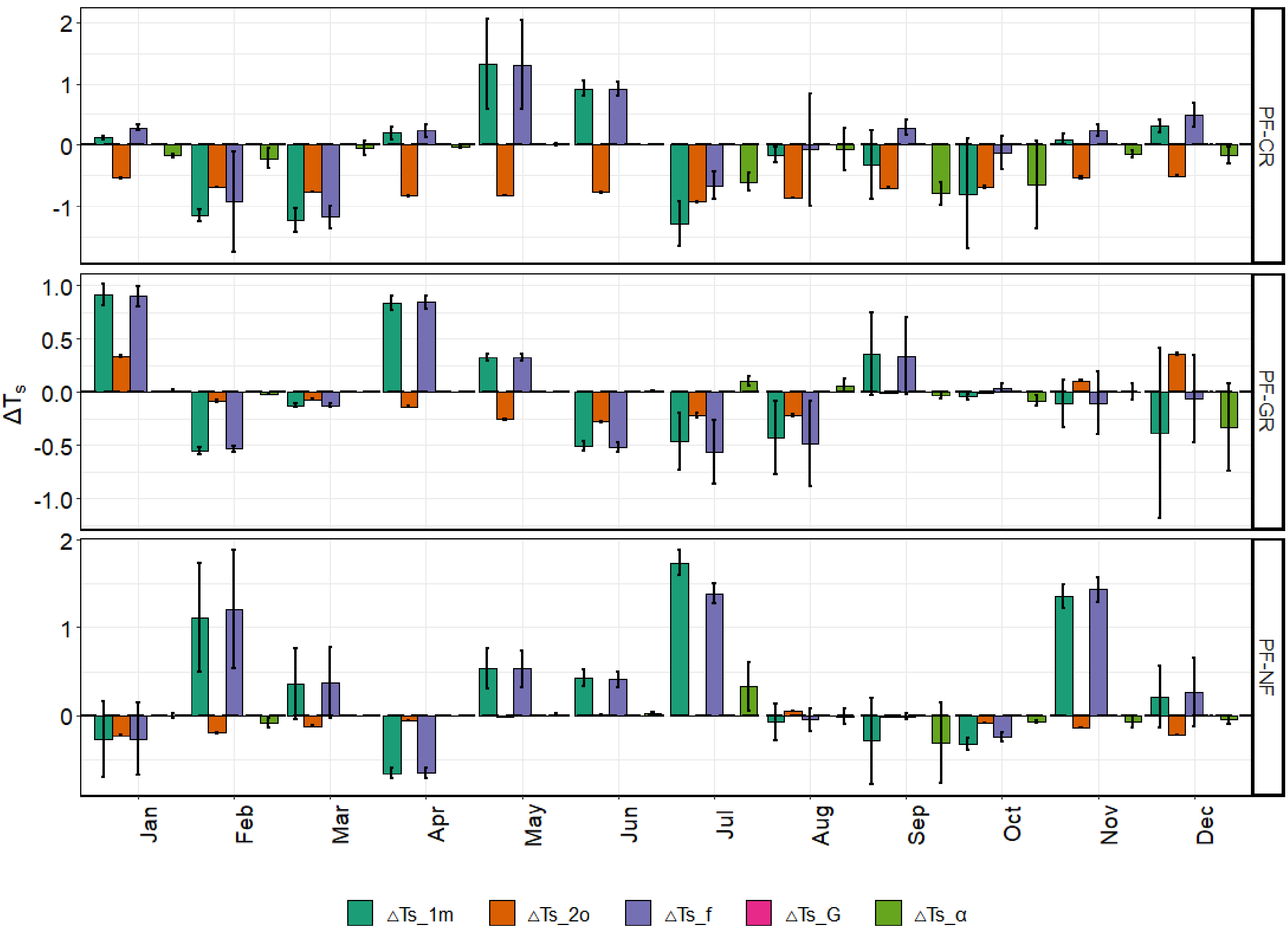

ΔTs
PF-CR
PF-GR
PF-NF
2
1
0
-1
1.0
0.5
0.0
-0.5
-1.0
Jan
Feb
Mar
Apr
May
Jun
Jul
Aug
Sep
Oct
Nov
Dec
△Ts_1m
△Ts_2o
△Ts_f
△Ts_G
△Ts_α

Figure 4.

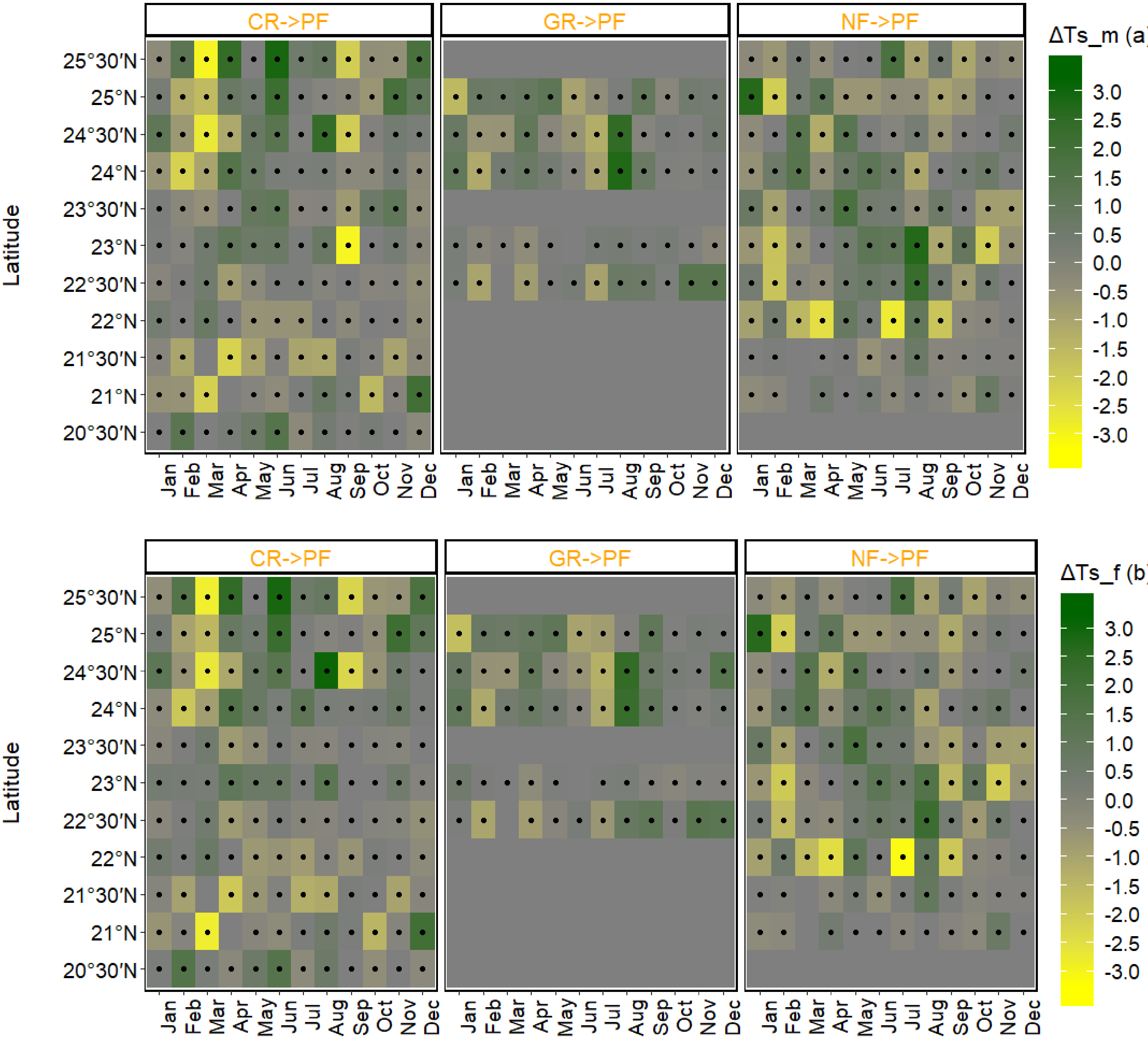
CR->PF
GR->PF
NF->PF
ΔTs_m (a)
ΔTs_f (b)
Latitude
25°30'N
25°N
24°30'N
24°N
23°30'N
23°N
22°30'N
22°N
21°30'N
21°N
20°30'N
Jan Feb Mar Apr May Jun Jul Aug Sep Oct Nov Dec
3.0 2.5 2.0 1.5 1.0 0.5 0.0 -0.5 -1.0 -1.5 -2.0 -2.5 -3.0

Figure 5.

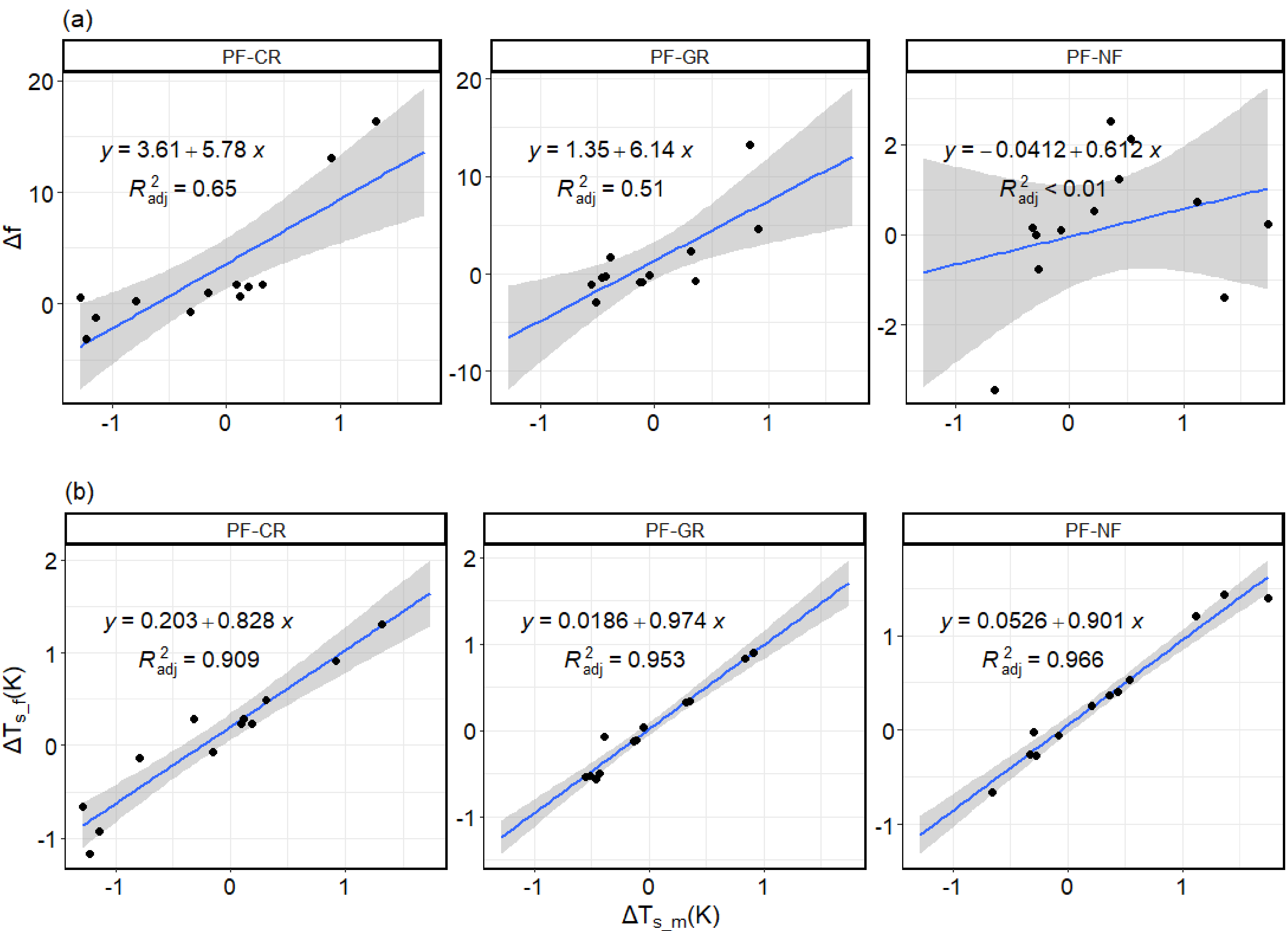

(a)
PF-CR
PF-GR
PF-NF
y = 3.61 + 5.78 x
R²adj = 0.65
y = 1.35 + 6.14 x
R²adj = 0.51
y = −0.0412 + 0.612 x
R²adj < 0.01
Δf
(b)
PF-CR
PF-GR
PF-NF
y = 0.203 + 0.828 x
R²adj = 0.909
y = 0.0186 + 0.974 x
R²adj = 0.953
y = 0.0526 + 0.901 x
R²adj = 0.966
ΔTs_f(K)
ΔTs_m(K)

Figure 6.

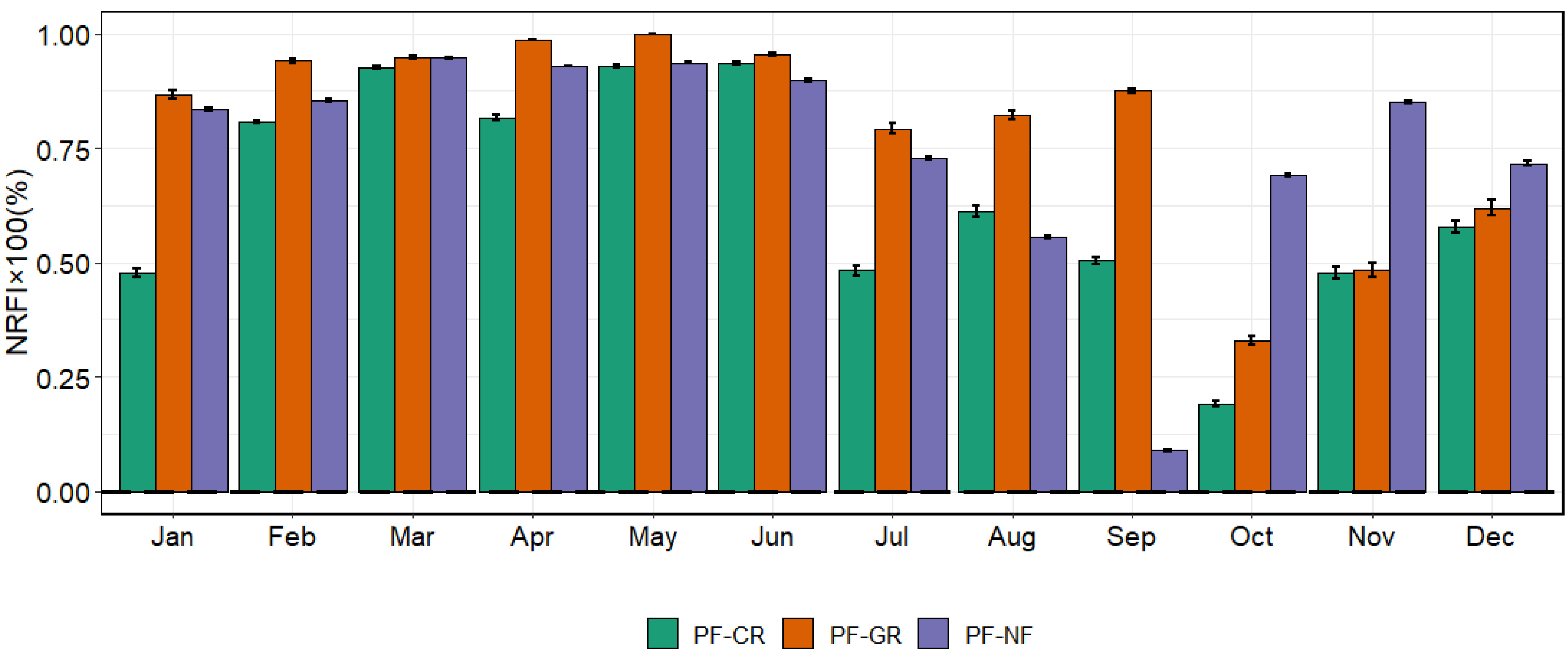

NRFI×100(%)
1.00
0.75
0.50
0.25
0.00
Jan
Feb
Mar
Apr
May
Jun
Jul
Aug
Sep
Oct
Nov
Dec
PF-CR
PF-GR
PF-NF